BASIC RESEARCH www.jasn.org

CKD Accelerates Development of Neointimal Hyperplasia in Arteriovenous Fistulas

Taku Kokubo,*† Noriyuki Ishikawa,*† Hisashi Uchida,*† Sara E. Chasnoff,† Xun Xie,† Suresh Mathew,‡ Keith A. Hruska,‡ and Eric T. Choi†§

*Department of Cardiovascular Surgery, Asahikawa Medical University, Hokkaido, Japan; †Department of Surgery, Washington University School of Medicine, St. Louis, Missouri; ‡Departments of Medicine and Pediatric, Renal Divisions, Washington University School of Medicine, St. Louis, Missouri; and §Department of Surgery, John Cochran VA Hospital, St. Louis, Missouri

ABSTRACT

Arteriovenous (AV) access failure resulting from venous neointimal hyperplasia is a major cause of morbidity in patients with ESRD. To understand the role of chronic kidney disease (CKD) in the development of neointimal hyperplasia, we created AV fistulae (common carotid artery to jugular vein in an end-to-side anastomosis) in mice with or without CKD (renal ablation or sham operation). At 2 and 3 wk after operation, neointimal hyperplasia at the site of the AV anastomosis increased 2-fold in animals with CKD compared with controls, but cellular proliferation in the neointimal hyperplastic lesions did not significantly differ between the groups, suggesting that the enhanced neointimal hyperplasia in the setting of CKD may be secondary to a migratory phenotype of vascular smooth muscle cells (VSMC). In *ex vivo* migration assays, aortic VSMC harvested from mice with CKD migrated significantly greater than VSMC harvested from control mice. Moreover, animals with CKD had higher serum levels of osteopontin, which stimulates VSMC migration. When we treated animals with bone morphogenic protein-7, which promotes VSMC differentiation, before creation of the AV anastomosis, the effect of CKD on the development of neointimal hyperplasia was eliminated. In summary, CKD accelerates development of neointimal hyperplasia at the anastomotic site of an AV fistula, and administration of bone morphogenic protein-7 neutralizes this effect.

J Am Soc Nephrol 20: 1236–1245, 2009. doi: 10.1681/ASN.2007121312

Arteriovenous (AV) access dysfunction such as stenosis and thrombosis constitute a major cause of morbidity for patients on chronic hemodialysis for end-stage kidney disease.[1] While AV fistulae constructed with native vessels are the best vascular access available owing to a lower incidence of stenosis, thrombosis, and infection compared with vascular grafts or central venous catheters, its failure rate up to 66% at 2 yr[2] remains unacceptably high as hemodialysis access related hospitalizations are on the rise and its cost are well over one billion dollars per annum in the United States alone.[3]

The cause of failure is predominantly secondary to the occlusive neointimal hyperplastic (NH) lesion formation at the anastomosis and/or the outflow veins followed by *in situ* thrombosis.[4–7] Unlike restenosis seen with preocclusive atherosclerotic arteries after angioplasty and stenting, neointimal (new intimal) hyperplasia is seen at the anastomosis involving an artery or a synthetic graft (*e.g.*, expanded polytetrafluoroethylene, or ePTFE, or Dacron) and a vein in the upper extremities. Although these blood vessels are predisposed to calcification, pre-existing NH, and needle stick injury, they are usually free of atherosclerotic plaque. Therefore, directional migration of vascular smooth muscle cells

Received December 10, 2007. Accepted January 28, 2009.

Published online ahead of print. Publication date available at www.jasn.org.

Correspondence: Dr. Eric T. Choi, 660 S. Euclid Avenue, Campus Box 8109, Saint Louis, Missouri 63110. Phone: 314-362-6490; Fax: 314-362-4615; E-mail: choie@wustl.edu

Table 1. Body weight, blood pressure, heart rate, and serum chemistry

	Sham (n = 8)	CKD (n = 10)	P value
Body weight (g)	27.5 ± 1.4	26.2 ± 1.0	NS
Blood pressure (mmHg)[a]			
Systolic	108.7 ± 5.4	99.8 ± 3.7	<0.002
Diastolic	77.1 ± 5.8	70.5 ± 5.2	<0.05
Mean	91.7 ± 5.2	84.1 ± 4.4	<0.02
Heart rate (per minute)[a]	553 ± 37	563 ± 38	NS
Chemistry			
BUN (mg/dl)	30.3 ± 4.8	57.6 ± 18.0	<0.001
Phosphorus (mg/dl)	8.3 ± 1.5	7.1 ± 1.0	NS
Calcium (mg/dl)	9.3 ± 0.5	9.4 ± 1.0	NS

Data are expressed as mean ± 1 SD.
[a]Separate animals were used: sham (n = 8) and CKD (n = 7).

(VSMCs) into the luminal surface is critical to the anastomotic NH lesion formation.[8,9]

Several animal models with native or synthetic graft accesses have been used to gain insight into the pathologic mechanisms of NH lesion development.[10,11] However, these studies lacked the critical component of chronic kidney disease (CKD), and whether CKD plays a role in NH lesion formation remains unknown. CKD has been implicated in the development of atherosclerosis along with a host of other deranged factors such as hemodynamic forces, inflammatory mediators, platelet activation, coagulation cascade, and metabolic factors.[12,13] In this study, we used a murine model of CKD modified from Gagnon and Gallimore,[14] to assess the effect of CKD on NH formation after AV fistula creation.

RESULTS

Creation of CKD and Sham Mice

After the AV fistula creation, CKD and sham mice underwent serum biochemical analyses (Table 1). There were no significant differences in the tested biochemical measurements except for the doubling of blood urea nitrogen (BUN) level in the CKD group compared with the sham group (30.3 ± 4.8 mg/dl versus 57.6 ± 18.0 mg/dl; $P < 0.002$). There were no significant differences in weight between the groups at the time of AV fistula creation (Table 1) and throughout the study (data not shown). We measured BP by catheter transducers under light isoflurane anesthesia. The CKD animals (n = 7) had significantly lower BP compared with sham animals (n = 8) (Table 1). Thus, our CKD mice were not hypertensive. Whether the decreased BP in the CKD mice was due to increased sensitivity to the anesthetic agent due to CKD cannot be established in these experiments. In contrast to our BP recordings, Gignon and Gallimore[14] used the tail-cuff technique and found no significant difference in BP between CKD and sham mice.

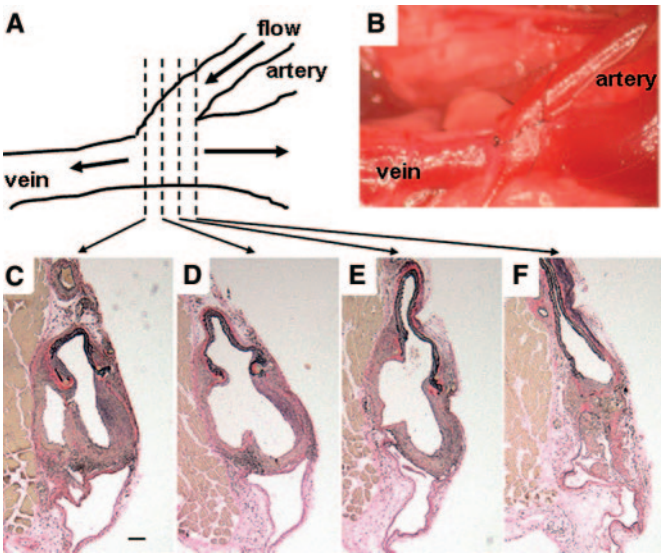

Figure 1. Schematic representation of the AV anastomosis. Drawing (A) and actual picture (B) of mouse model of AV fistula creation with anastomosis of end left common carotid artery to side left external jugular vein. One hundred-micrometer cross-sections of the venous anastomosis 3 wk following AV fistula creation (C to F). Scale bar, 100 μm.

CKD and NH Formation after AV Fistula Creation

Ten CKD and eight sham mice underwent the AV fistula creation (Figure 1A,B) and survived 3 wk for the histomorphometric analyses. We made serial sections every 100 μm throughout the AV anastomosis, and we observed uniform NH lesion and thrombus formation at the anastomotic site (Figure 2). We identified the NH lesion by immunohistochemical staining for SM-specific α-actin (Figure 2, B, C, E, and F). The NH lesion volume at the anastomosis of the CKD group was 2-fold greater than that of the sham group (Figure 2G;

Table 2. Time course of anastomotic NH lesion and thrombus formation after the creation of AV fistula in sham and CKD mice

	Mice	1 wk (sham, n = 6) (CKD, n = 8)	2 wk (sham, n = 8) (CKD, n = 10)	3 wk (sham, n = 8) (CKD, n = 10)
NH lesion volume (mm^3)	Sham	0.038 ± 0.033	0.044 ± 0.012	0.048 ± 0.028
	CKD	0.014 ± 0.007	0.136 ± 0.073[a]	0.107 ± 0.036[b]
Thrombus volume (mm^3)	Sham	0.032 ± 0.019	0.056 ± 0.024	0.095 ± 0.077
	CKD	0.094 ± 0.090	0.081 ± 0.053	0.063 ± 0.034

Data are expressed as mean ± 1 SD.
[a]$P < 0.01$ versus sham at 2 wk.
[b]$P < 0.005$ versus sham at 3 wk.

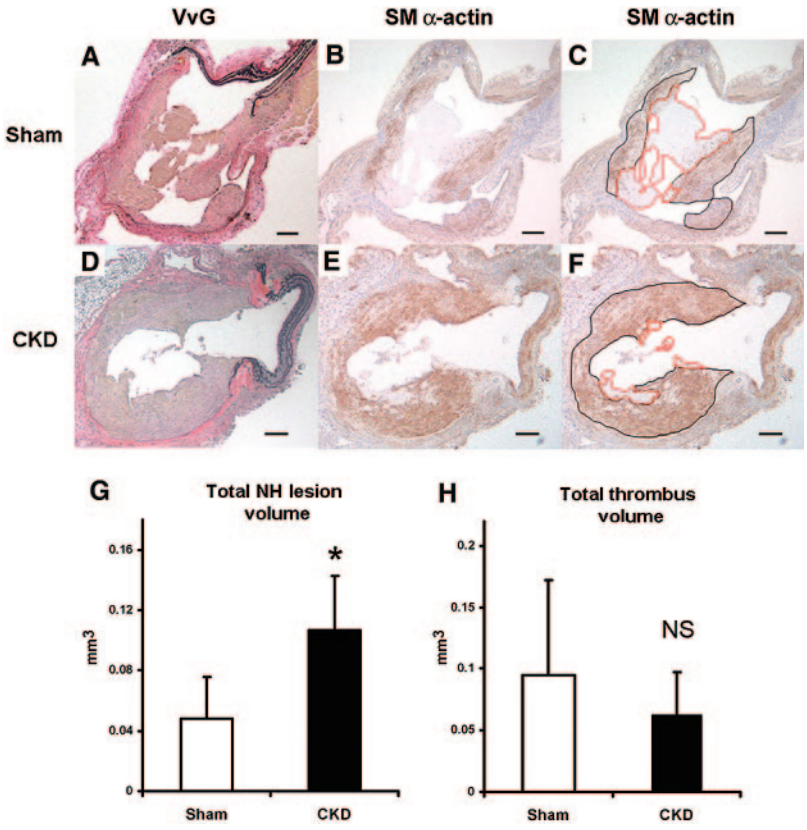

Figure 2. NH lesion and thrombus measurements at the AV fistula anastomosis. Representative cross-sections of the venous anastomosis from sham (A to C) and CKD (D to F) mice at 3 wk after the creation of AV fistula. NH lesions were stained for elastin (VvG) (A and D) and SMCs (SM-specific α-actin) (B, C, E, and F) to identify SMCs (stained brown). SM-specific α-actin stainings show the NH lesions (black border) and the thrombus lesions (red border) of AV fistula in sham mice (C) and CKD (F). Scale bar, 100 μm in panels A to F. The total anastomotic NH lesion volume was significantly different between the sham ($n = 8$) and CKD ($n = 10$) mice (panel G, $^*P < 0.01$). There was no significant difference (NS) in thrombus volume (H) at the anastomosis between sham and CKD mice. Error bars, 1 SD.

$^*P < 0.01$). There were no significant differences in the thrombus volume between CKD and sham groups (Figure 2H; NS).

CKD Mice Do Not Have a Shortened Time to Thrombosis

To determine whether vascular injury leading to thrombosis was the mechanism by which CKD stimulated NH lesion development, we used laser-induced occlusion of the carotid artery in CKD and sham mice. Figure 3,A and B, compare the time to thrombus formation after photochemical injury of the common carotid artery of CKD and sham animals. In CKD animals, the occlusion time was 97 $\pm$ 34 min (mean $\pm$ SD) compared with 48 $\pm$ 14 min for sham animals ($P < 0.005$). Therefore, CKD inhibits injury-induced thrombosis demonstrating that CKD-

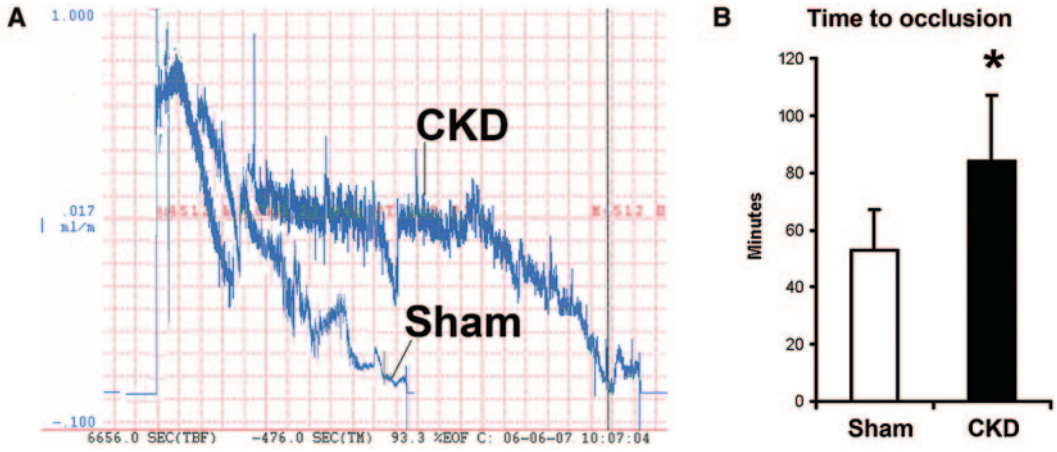

Figure 3. Effect of CKD on thrombotic occlusion of the carotid artery. Blood flow in the common carotid artery was monitored continuously with an ultrasonic flow probe. Local endothelial injury was induced by application of a 540-nm laser beam to the carotid artery followed by injection of rose bengal dye (50 mg/kg) into the lateral tail vein. (A) Representative blood flow recordings showing the delayed occlusion time and stochastic flow pattern in CKD and sham animals. Rose bengal dye was injected at time = 0 min. (B) The time to occlusion of blood flow following injury is shown, and CKD animals had a significantly longer time to thrombus formation and arterial occlusion as compared with the sham animals. Error bars, 1 SD ($n = 8$ for each group). $^*P < 0.01$.

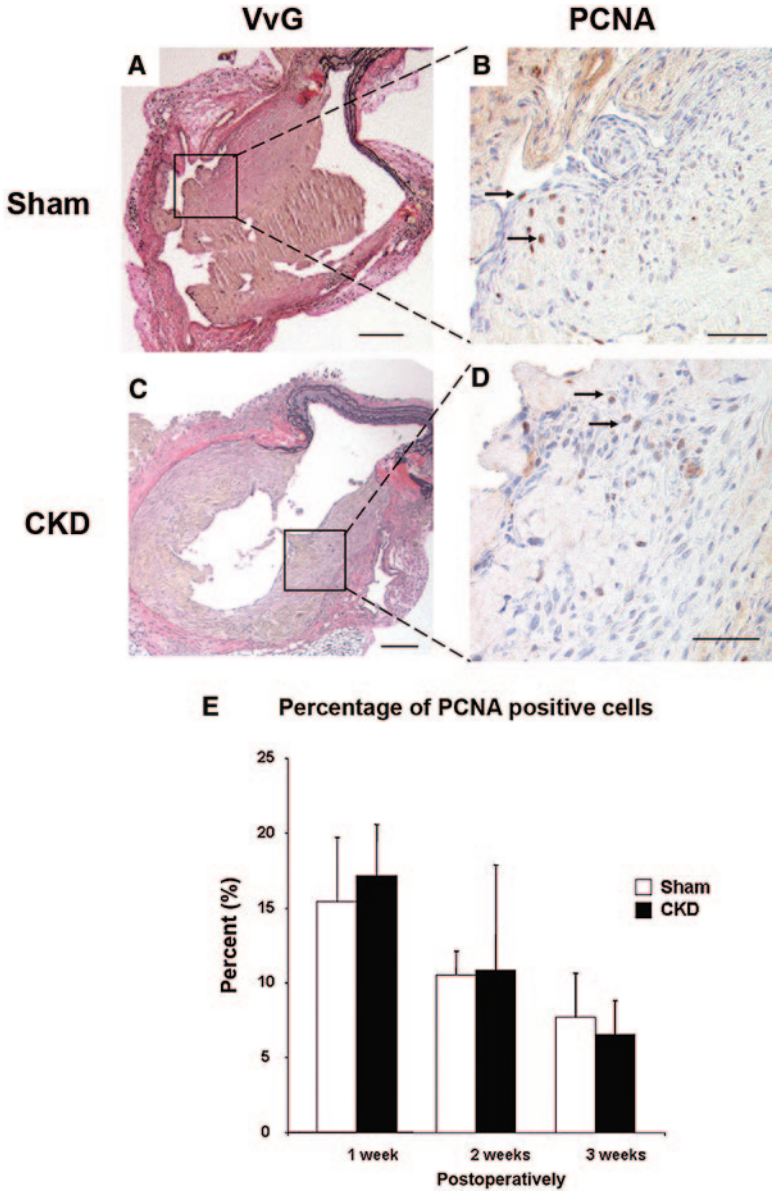

Figure 4. Percentage of PCNA positive cells in the CKD and sham NH lesions at 1, 2, and 3 wk postoperatively. Representative cross-sections of the venous anastomosis from sham (A and B) and CKD (C and D) mice at 3 wk after the AV fistula creation. NH lesions were stained for elastin (VvG) (A and C) and PCNA (B and D) to identify proliferating SMCs (arrows, nuclei stained brown). Scale bar, 100 μm in panels A and C. Scale bar, 25 μm in panels B and D. There were no significant differences in the percentage of PCNA positive cells in the NH lesions between the sham and CKD mice at 1 wk (sham, $n = 5$ mice and CKD, $n = 5$ mice), 2 wk (sham, $n = 5$ and CKD, $n = 5$) and 3 wk (sham, $n = 8$ and CKD, $n = 10$) postoperatively (E). Error bars, one SD.

stimulated NH formation is not associated with increased thrombus formation at the anastomotic site.

SMC Proliferation at 1, 2, and 3 Weeks Postoperation

To determine the role of SMC proliferation in the CKD-enhanced NH development, we created AV fistula in additional sham and CKD mice and harvested AV fistula specimens at 1 and 2 wk postoperatively in addition to the 3-wk time point from the above experiments. Using proliferating cell nuclear antigen (PCNA) staining, we determined that despite the enhanced NH lesion formation in CKD mice, there were no differences in the cellular proliferation rate in the NH lesion between the sham and CKD mice at all time points (Figure 4). The NH lesion and thrombus volumes in these mice are shown in Table 2. The NH lesion was increased at 2 and 3 wk postoperatively with no differences in the thrombus volume at all time points.

Minimal Bone Marrow Contribution in NH

To determine if the bone marrow contributes to the NH lesion formation, we performed total body irradiation on transgenic mice with green-fluorescence protein (GFP) and wild-type (WT; C57Bl/6 background) mice followed by reconstitution with WT and GFP mouse bone marrow, respectively. Six weeks later, two groups of animals ($n = 5$ per group) underwent renal ablation procedure (CKD) followed by AV fistulae creation. Three-weeks after the AV fistula creation, all GFP CKD mice reconstituted with WT bone marrow ($BMT^{WT \rightarrow GFP}$) had fluorescence detected throughout the NH lesion (Figure 5A, C, and E), while all WT CKD mice reconstituted with GFP bone marrow ($BMT^{GFP \rightarrow WT}$) had minimal fluorescence detected in the similarly prominent NH lesion, suggesting that the bone marrow does not contribute significantly to the lesion formation in the setting of AV fistula (Figure 5, B, D, and F).

CKD Increases SMC Motility in *Ex Vivo* Invasion Assay

Aortic explants were used to study the effects of CKD on VSMC motility. Autologous CKD and normal sera, respectively, were used as motility stimulants. By day 7, a dense cloud of VSMC surrounded the CKD aortic explant with the leading front of the advancing VSMC having migrated >1000 μm in collagen (Figure 6B). In contrast, there was minimal VSMC surrounding the normal aortic explant (Figure 6A), demonstrating that CKD increases VSMC migration away from the aortic explant in this assay. Even in the setting of lack of cellular proliferation with 5 mM hydroxylurea, CKD increased VSMC motility (Figure 6, C and D).

Osteopontin Level Is Elevated in the CKD Mice

Lack of difference in the cellular proliferation at the anastomosis in CKD and sham animals suggests that accelerated cellular migration into the anastomosis resulting in enhanced NH formation may be occurring in CKD animals.

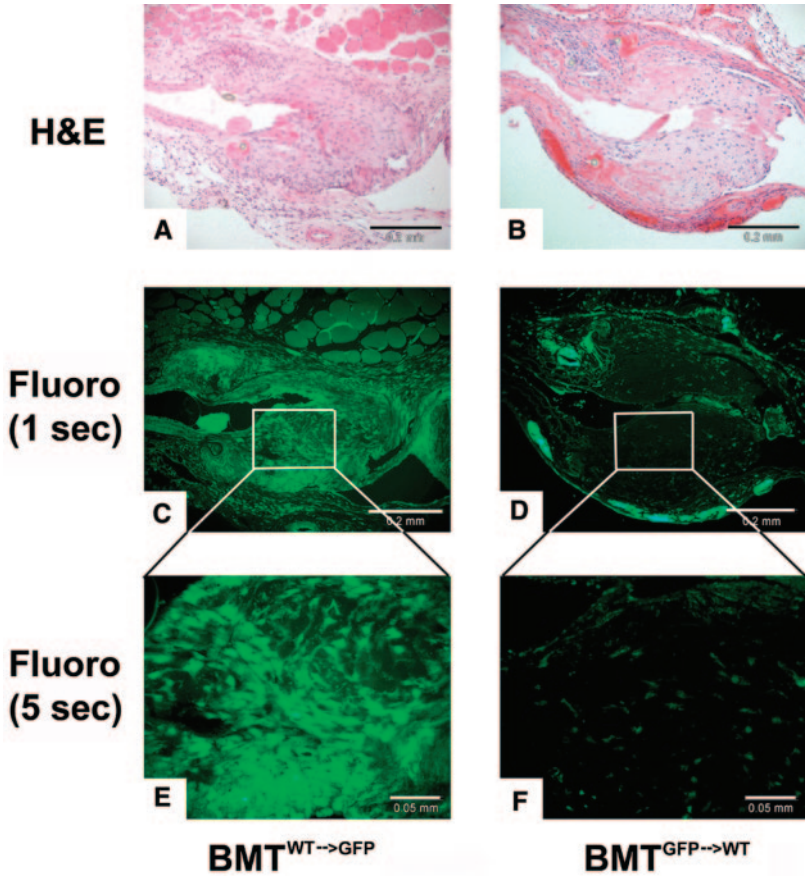

Figure 5. Bone marrow contribution to the NH lesion was examined by lethal total body irradiation of GFP and wild-type mice followed by GFP bone marrow reconstitution ($BMT^{WT \rightarrow GFP}$ versus $BMT^{GFP \rightarrow WT}$) and renal ablation. (A and B) Six weeks after bone marrow reconstitution, renal ablation was performed, and an AV fistula was created. Three weeks later, venous anastomoses were sectioned and stained for H&E (scale bar, 0.02 mm). (C) Fluorescence detected at 1 s of $BMT^{WT \rightarrow GFP}$ demonstrated that GFP is densely present in the neointima (scale bar, 0.02 mm). (D) However, fluorescence detected at 1 s of $BMT^{GFP \rightarrow WT}$ demonstrated that GFP is not detected in the NH lesion and only in the adventitia, suggesting that bone marrow-derived cells do not contribution to the make-up of the NH lesions (scale bar, 0.2 mm). (E and F) Higher magnification with 5 s of fluorescence (scale bar, 0.05 mm).

Indeed, we have shown that $\alpha_v\beta_3$ integrin receptor expressed on VSMC stimulated by matrix components, such as osteopontin (OPN), is critical to cellular migration and NH lesion formation after arterial injury.[15] Moreover, Natta and colleagues[16] reported that plasma concentration of soluble OPN was significantly higher in patients with ESRD compared with their healthy counterparts. Therefore, we measured the serum level of soluble OPN in CKD and sham mice and found that the OPN level was significantly higher in CKD mice than that of sham mice (1103 $\pm$ 327 ng/ml versus 897 $\pm$ 209 ng/ml; $P < 0.01$) (Figure 7). To determine if this elevation of OPN level in the setting of CKD is the culprit for the larger anastomotic NH lesion, we used OPN-deficient ($OPN^{-/-}$) and WT ($OPN^{+/+}$) mice to test the hypothesis. These animals underwent CKD and AV fistula creation as described previously. Three weeks later, we sacrificed the animals and harvested and analyzed the AV anastomoses. There was no significant difference between the $OPN^{-/-}$ and $OPN^{+/+}$ mice in CKD stimulation of the NH lesion, suggesting that elevated OPN level associated with CKD was not the mechanism of NH lesion stimulation or that the sensitivity of our test system missed the OPN effect.

Bone Morphogenic Protein-7 Treatment Neutralizes the Effect of CKD on NH

To study the possibility that CKD induced VSMC dedifferentiation allowing higher rates of migration, we examined the effects of a systemically administered VSMC differentiation factor[17,18] on NH lesion development. Mice underwent CKD creation, and 3 wk later underwent AV fistula creation. One week before the AV fistula creation and continuing through to AV anastomosis harvest, we administered 100 μg/kg bone morphogenic protein-7 (BMP-7) or its vehicle (saline) intraperitoneally twice a week. In sham operated animals, there was no effect of BMP-7 on NH lesion development (Figure 8), but BMP-7 administration eliminated the stimulation of NH lesion formation induced by CKD (Figure 8).

DISCUSSION

The present study demonstrates that CKD has a profound effect on the development of NH at the anastomosis in a murine model of AV fistula. Three weeks after the creation of an AV fistula, CKD mice had a 2-fold increase in the total NH volume compared with the sham animals with normal kidney function. As far as we know, this is the first demonstration of the role of CKD in the development of NH in an animal model. These data support the hypothesis that CKD leads to accelerated NH formation, the primary cause of AV access failure in the chronic hemodialysis patient population.

The impact of CKD on NH lesion development cannot be

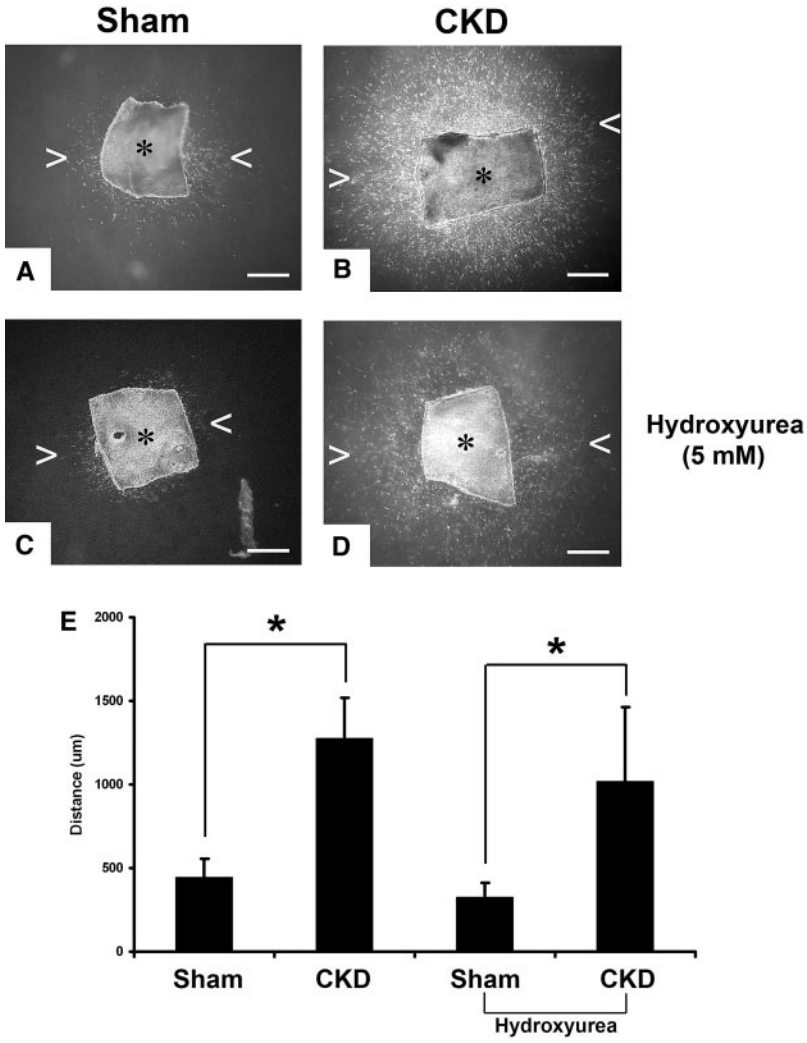

Figure 6. *Ex vivo* migration activity of VSMCs in three-dimensional collagen. (A and B) CKD and sham media explants of mouse aorta were embedded within a three-dimensional gel of type I collagen, and VSMC migration from the explants were initiated from CKD and sham sera, respectively. Outgrowth into the translucent collagen matrix was visualized by darkfield microscopy at 7 d. Asterick (*) indicates explant, and arrowheads (< and >) point at the leading edge of the migrating VSMC (scale bar, 500 μm). (C and D) Same assays are performed with the addition of 5 mM hydroxyurea resulting in absence of cellular proliferation. (E) CKD stimulated significantly more VSMC migration as determined by the leading edge away from the explants ($n = 8$ aortic explants per group). *$P < 0.01$.

measured in humans, because we do not create AV fistulae in healthy subjects. However, we do have some insight into the effect of CKD on bypass grafts. Much like the primary cause of failure in hemodialysis AV grafts and fistulae in the upper extremities, stenosis due to NH is a major reason for failure of bypass grafts (*e.g.*, synthetic grafts and autologous veins) in the lower extremities.[19,20] For instance, the patency rates for lower extremity bypass grafts are 40% to 78% in 3 yr in the general population,[21–23] but the patency rates of bypass grafts in CKD patients is significantly less[24,25] approaching the patency rates of 17% to 34% at 2 yr associated with hemodialysis AV grafts and fistulae.[2] While our animals (stage 3 to 4 CKD) did not have end stage kidney disease, the anastomotic NH lesions in our murine model have the characteristics of the occlusive NH lesions found in human hemodialysis AV fistula. Therefore, the data from our mouse CKD model of AV fistula may provide useful insights into the effect of CKD on anastomotic NH.

Creation of AV fistulae in CKD and sham mice demonstrated that CKD accelerates NH lesion development in AV fistulae. PCNA staining of the NH lesions demonstrated that there were no differences in cellular proliferation rates in the NH lesions between the sham and CKD mice. The overwhelming cell type in the NH lesions was the VSMC (Figure 4) with minimal number of inflammatory cells (data not shown). There was also minimal cellular contribution from the bone marrow as demonstrated by GFP bone marrow transplantation (Figure 5). We found that CKD mice had significantly higher rates of VSMC motility stimulated by its serum and that the serum levels of soluble OPN were increased in CKD mice compared with those of sham mice. OPN is a potent migratory agent for VSMC.[26–28] Indeed, Nitta and colleagues[16] showed that patients with ESRD have significantly higher levels of soluble OPN compared with their healthy counterparts, which is in agreement with our results in the CKD mice. However, OPN deficiency did not affect the stimulation of the NH lesion size associated with CKD.

The stimulation of VSMC migration by CKD suggests an effect on differentiation allowing a switch from a contractile to a migratory phenotype. Recently, CKD has been shown to accelerate atherogenesis and stimulate dedifferentiation of VSMC migrating into the neointima in apolipoprotein E knockout mice, which develop hypercholesterolemia as a re-

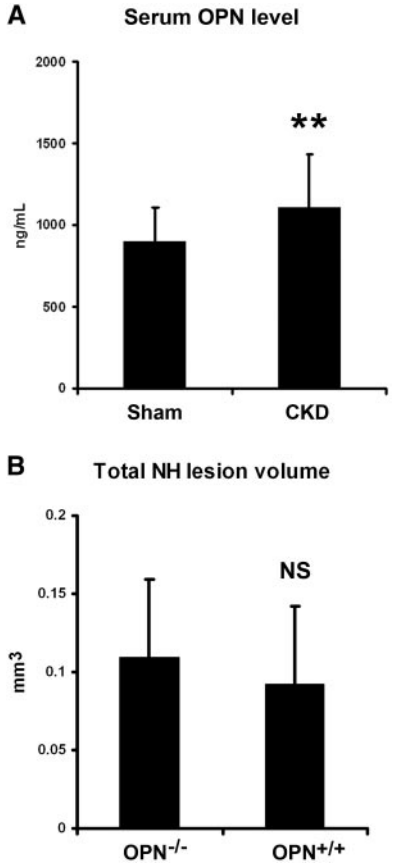

Figure 7. CKD effect on NH lesion development persists in OPN-deficient mice. (A) Serum levels of OPN were measured in CKD ($n = 10$) and sham ($n = 8$) animals. CKD animals had a significantly higher OPN level than that of the sham animals (**$P < 0.05$). (B) Six weeks after CKD creation and 3 wk after AV fistula creation, there was no significant difference between the $OPN^{-/-}$ and $OPN^{+/+}$ mice in anastomotic NH lesion size. NS.

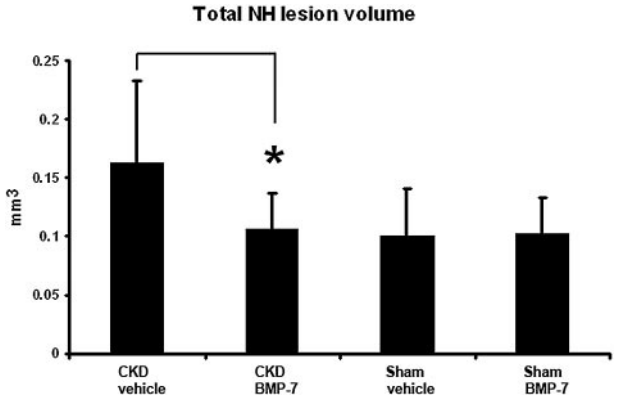

Figure 8. Effect of BMP-7 administration on CKD induction anastomotic NH lesion formation. Animals underwent CKD creation, and 3 wk later underwent AV fistula creation. One week before the AV fistula creation and continuing through to AV anastomosis harvest, BMP-7 was administered intraperitoneally twice a week with a dose of 100 μg/kg. In sham operated animals, there was no effect of BMP-7 on NH lesion size (18 BMP-7 animals versus 16 vehicle animals). However, BMP-7 administration eliminated the stimulation of NH lesion formation induced by CKD (16 BMP-7 animals versus 19 vehicle animals). *$P < 0.01$.

sult of an accumulation of chylomicron remnants, VLDL, and intermediate-density lipoproteins,[13,29,30] and in LDL receptor knockout ($LDLR^{-/-}$) mice.[31,32] These abnormalities of VSMC differentiation may relate to the abnormalities of VSMC function in the present study. To examine this possibility, a VSMC differentiation factor, BMP-7,[17,18] was administered. Indeed, BMP-7 therapy blocked the CKD stimulation of the NH lesion. This is consistent with the possibility that the CKD-stimulated VSMC migration to the NH lesion was allowed through effects of CKD to diminish the VSMC differentiation of the migrating cells. Consistent with this concept, we have shown that CKD stimulates osteoblastic differentiation of aortic neointimal SMCs in the $LDLR^{-/-}$ high-fat fed mice[32] and that the CKD effect was prevented by BMP-7.[33,34] In agreement with Dorai *et al.*,[17,18] we have shown that BMP-7 stimulates expression of markers of the VSMC contractile phenotype *in vitro* [35] and suppresses expression of the osteoblastic phenotype *in vitro* and *in vivo*.[32] Since the data on markers of the VSMC contractile phenotype are from a model that differs from those used in this manuscript, they are provided in supplementary form (Supplemental Figure S1). Experiments analyzing the effects of CKD on differentiation of VSMC in the models used in this manuscript are beyond its scope, as they require development of new culture models. In summary, we have established a model of AV fistulae in the mouse complicated by the NH lesion. CKD increases the NH lesion through increased VSMC motility, which was inhibited by a stimulus to VSMC differentiation. We believe that this model will be useful in further dissecting the mechanisms involved in the development of anastomotic NH.

CONCISE METHODS

Mice

All procedures were approved by the Animal Studies Committee at Washington University and conform to the *Guide for the Care and Use of Laboratory Animals* published by the United States National Institutes of Health (NIH Publication No. 85 to 23, 1996). We purchased OPN-deficient ($OPN^{-/-}$) and its WT mice ($OPN^{+/+}$; background, C57BL/6 mice) and GFP[36] and its WT mice (background, C57BL/6 mice) from The Jackson Laboratory (Bar Harbor, Maine). Otherwise, we used C57BL/6 mice for the remaining CKD experiments. We used only 10- to 16-wk-old male mice in the study. They were housed in polycarbonate cages in a pathogen-free, temperature-controlled environment with free access to a standard chow diet and water.

Creation of CKD and Sham Mice

We used a two-step renal ablation procedure to create CKD mice as described previously in our laboratories.[14,31] Briefly, we applied cortical electrocautery to the right kidney of 10- to 12-wk-old mice through a 2-cm flank incision and performed total left nephrectomy 2

wk later. Sham control animals received sham operations that included decapsulation of both kidneys. Six weeks later, the animals underwent AV fistula creation. All AV fistulae were patent by inspection at the time harvest and confirmed by histology and used for the data analyses.

BP Measurement

Mice were anesthetized with 1.5% isoflurane inhaled through a nose cone and kept warm by radiant heat. We inserted a catheter (Millar Instruments, Houston, Texas) into the right common carotid artery and monitored BP for 20 min. We reduced the isoflurane concentration to 0.5% during this period for at least 5 min, and we recorded the average heart rate and systolic, diastolic, and mean pressures.

Creation of AV Fistula

Animals underwent an AV fistula creation by anastomosing the left common carotid artery to the jugular vein in an end-to-side fashion. Under a sterile condition, we made a vertical incision in the left neck with the left common carotid artery and carefully dissected out the adjacent external jugular vein. We placed the common carotid artery clamp at the proximal portion with an 11-0 nylon suture and divided the common carotid artery just proximal to the bifurcation. Next, we clamped the jugular vein proximally and distally and punctured it in the middle portion with a 27-gauge syringe. After filling this vein segment with heparinized saline, we performed the venotomy of 0.7 mm in length. Then we created the end-to-side anastomosis (common carotid artery end to jugular vein side) using 11-0 nylon heel-to-toe continuous suturing. We unclamped the vessels and checked for patency (Figure 1, A and B).

Three weeks after AV fistula creation, we euthanized the animals, and the AV anastomoses were perfusion-fixed via the left ventricle at 100 mmHg pressure as described previously.[37] Before perfusion fixation, we drew blood from the left ventricle for the biochemical analysis. BUN, phosphorus, and calcium were measured by autoanalyzer techniques in the Animal Facility Clinical Laboratory at Washington University in St. Louis, Missouri. We measured mouse serum OPN levels with a commercially available enzyme-linked immunosorbent assay (ELISA) kit purchased from Assay Designs, Ann Arbor, Michigan.

Immunohistochemistry and Histomorphometry

We harvested the jugular vein and the left common carotid artery adjacent to the anastomosis at the time of sacrifice. Samples were processed and embedded in paraffin. We obtained serial sections of 5-μm thickness every 100 μm throughout the AV anastomosis (Figure 1, C to F) or the entire left common carotid artery (ligation injury), and we stained them with Verhoeff elastic-van Gieson (VvG) and hematoxylin and eosin (H&E).[15] For immunohistochemistry, adjacent sections were stained for SMC (SM α-actin, 1:500 dilution; Sigma-Aldrich, St. Louis, Missouri) and PCNA (1:1000 dilution; Santa Cruz Biotech, Santa Cruz, California) as described previously.[15]

We performed volumetric measurements for NH lesion and thrombus on digitizing images using Olympus Microsuite software (Olympus Soft Imaging Solutions, Lakewood, Colorado). First, we determined the luminal border of the anastomosis with VvG staining of the internal elastic lamina. Second, SMCs and surrounding extracellular matrix stain could be distinguished from thrombus with nuclear and collagen staining of H&E and overlapping staining of SM-specific α-actin. Inflammatory cells (neutrophils and macrophages) and thrombus did not stain for SM-specific α-actin (brown) and collagen (pink on H&E).

All anastomoses had four to five 100-μm sections. We used all sections, including the anastomotic and peri-anastomotic segments, to determine the total anastomotic NH lesion volume. We easily identified the NH lesion borders by the lumen and the internal elastic lamina and the cells staining for SM-specific α-actin. We calculated the total NH lesion volume with the summation of consecutive sections and multiplied them by 100 μm (distance between sections). Similarly, we calculated the anastomotic and peri-anastomotic thrombus volume from each cross-section and compared them between CKD and sham animals.

Cellular Proliferation Rate Calculation

The PCNA technique is as described previously in our laboratory.[15] In short, we selected two adjacent anastomotic cross-sections with the largest NH lesion formation from every CKD and sham animal harvested at 1, 2, and 3 wk after fistula creation. We counted all of the nuclei (denominator) in the NH lesion with H&E staining and counted the nuclei stained for PCNA (nominator) to determine the percentage of cellular proliferation (mean $\pm$ SD). We then compared the percentage of proliferation between CKD and sham animals at each time point.

Photochemically Induced Carotid Artery Thrombosis in Mice

We followed the protocol of Eitzman *et al.*[38] with slight modification.[39] The CKD and sham animals were anesthetized with pentobarbital, secured in the supine position, and placed under a dissecting microscope. Following a midline cervical incision, the right common carotid artery was isolated, and we applied a Doppler flow probe (model 0.5 VB; Transonic Systems, Ithaca, New York). We induced thrombosis by an injection of rose bengal dye (Fisher Scientific, Pittsburgh, Pennsylvania) into the tail vein in a volume of 120 μl at a concentration of 50 mg/kg using a 29-gauge needle. Just before injection, we applied a 1.5 mW, 540 nm green light laser (Melles Griot, Carlsbad, California) to the desired site of injury from a distance of 6 cm. The laser remained on until thrombosis occurred. We monitored flow in the vessel with the Doppler probe for 150 min from the onset of injury, at which time the animal was humanely killed.

Irradiation and Bone Marrow Transplantation with GFP Mouse

GFP mouse are transgenic mice that ubiquitously express enhanced GFP.[36] GFP and wild-type (C57BL/6) mice underwent lethal gamma irradiation (approximately 9.5 Gy) from a cesium source, followed 6 h later by transplantation with femoral bone marrow cells obtained from 10-wk-old GFP donors (5×10^6 cells per recipient; 0.3 to 0.5 ml volume by retro-orbital injection) as described previously. [15] The animals were housed in a specific pathogen-free barrier environment.

All nontransplanted mice died 7 to 14 d after irradiation. After 6 wk, animals achieving successful bone marrow transplantation underwent renal ablation and AV fistula creation. Three weeks later, we sacrificed the animals for histomorphometric analyses.

Ex Vivo VSMC Migration Assay

Type I collagen acid extracted from rat tail tendons (Sigma-Aldrich) was dissolved in 0.2% acetic acid to a final concentration of 2.7 mg/ml.[40] Before the assay, fragments of mouse thoracic aorta from CKD and sham mice were stripped of intima and adventitia, and the media of the vessel wall was dissected into 1 × 1-mm fragments. Media explants from CKD and sham mice were then suspended within a solution of type I collagen and were cultured for 7 d in Dulbecco's modified Eagle's medium supplemented with 20% autologous CKD and sham mouse sera, respectively. We quantified migratory activity by measuring the distance migrated by the leading front of VSMC from the explanted tissue. For proliferation-free VSMC migration, we added 5 mM hydroxyurea to the media.

Statistical Analysis

Results are shown as mean ± one SD. Excel 2003 statistical package was used for the quantitative analysis of parameters such as NH lesion and thrombus volume (*t* test). *P* values less than 0.05 were considered significant.

ACKNOWLEDGMENTS

Oral presentation of this report was given at the American Society of Nephrology meeting (Renal week 2007), October 31-November 5, 2007, San Francisco, California. This research was supported in part by National Institutes of Health grant HL-68119 (to E.T.C.), by Grant-in-Aid from AHA Heartland Affiliate, Inc. (to E.T.C.), and by the Wylie Scholar Award (to E.T.C.) from the Pacific Vascular Research Foundation. Dr. Choi is affiliated with the John Cochran Veterans Administration Hospital in St. Louis, Missouri. We want to thank Dr. Douglas Tollefsen, Dr. Robert Mecham, and Mr. Russell Knutsen for their assistance with carotid occlusion experiments and BP measurements.

DISCLOSURES

None.

REFERENCES

1. Rotmans JI, Pasterkamp G, Verhagen HJ, Pattynama PM, Blankestijn PJ, Stroes ES: Hemodialysis access graft failure: Time to revisit an unmet clinical need? *J Nephrol* 18: 9–20, 2005
2. Shenoy S, Miller A, Petersen F, Kirsch WM, Konkin T, Kim P, Dickson C, Schild AF, Stewart L, Reyes M, Anton L, Woodward RS: A multicenter study of permanent hemodialysis access patency: Beneficial effect of clipped vascular anastomotic technique. *J Vasc Surg* 38: 229–235, 2003
3. Lee H, Manns B, Taub K, Ghali WA, Dean S, Johnson D, Donaldson C: Cost analysis of ongoing care of patients with end-stage renal disease: The impact of dialysis modality and dialysis access. *Am J Kidney Dis* 40: 611–622, 2002
4. Mattana J, Effiong C, Kapasi A, Singhal PC: Leukocyte-polytetrafluoroethylene interaction enhances proliferation of vascular smooth muscle cells via tumor necrosis factor-alpha secretion. *Kidney Int* 52: 1478–1485, 1997
5. Ezzahiri R, Lemson MS, Kitslaar PJ, Leunissen KM, Tordoir JH: Haemodialysis vascular access and fistula surveillance methods in The Netherlands. *Nephrol Dial Transplant* 14: 2110–2115, 1999
6. Cinat ME, Hopkins J, Wilson SE: A prospective evaluation of PTFE graft patency and surveillance techniques in hemodialysis access. *Ann Vasc Surg* 13: 191–198, 1999
7. Tordoir JH, Hofstra L, Leunissen KM, Kitslaar PJ: Early experience with stretch polytetrafluoroethylene grafts for haemodialysis access surgery: Results of a prospective randomised study. *Eur J Vasc Endovasc Surg* 9: 305–309, 1995
8. Roy-Chaudhury P, Sukhatme VP, Cheung AK: Hemodialysis vascular access dysfunction: A cellular and molecular viewpoint. *J Am Soc Nephrol* 17: 1112–1127, 2006
9. Nikkari ST, Clowes AW: Restenosis after vascular reconstruction. *Ann Med* 26: 95–100, 1994
10. Castier Y, Lehoux S, Hu Y, Foteinos G, Tedgui A, Xu Q: Characterization of neointima lesions associated with arteriovenous fistulas in a mouse model. *Kidney Int* 70: 315–320, 2006
11. Johnson MS, McLennan G, Lalka SG, Whitfield RM, Dreesen RG: The porcine hemodialysis access model. *J Vasc Interv Radiol* 12: 969–977, 2001
12. Russell JC, Proctor SD: Small animal models of cardiovascular disease: Tools for the study of the roles of metabolic syndrome, dyslipidemia, and atherosclerosis. *Cardiovasc Pathol* 15: 318–330, 2006
13. Bro S, Bentzon JF, Falk E, Andersen CB, Olgaard K, Nielsen LB: Chronic renal failure accelerates atherogenesis in apolipoprotein E-deficient mice. *J Am Soc Nephrol* 14: 2466–2474, 2003
14. Gagnon RF, Gallimore B: Characterization of a mouse model of chronic uremia. *Urol Res* 16: 119–126, 1988
15. Choi ET, Khan MF, Leidenfrost JE, Collins ET, Boc KP, Villa BR, Novack DV, Parks WC, Abendschein DR: Beta3-integrin mediates smooth muscle cell accumulation in neointima after carotid ligation in mice. *Circulation* 109: 1564–1569, 2004
16. Nitta K, Ishizuka T, Horita S, Hayashi T, Ajiro A, Uchida K, Honda K, Oba T, Kawashima A, Yumura W, Kabaya T, Akiba T, Nihei H: Soluble osteopontin and vascular calcification in hemodialysis patients. *Nephron* 89: 455–458, 2001
17. Dorai H, Vukicevic S, Sampath TK: Bone morphogenetic protein-7 (osteogenic protein-1) inhibits smooth muscle cell proliferation and stimulates the expression of markers that are characteristic of SMC phenotype in vitro. *J Cell Physiol* 184: 37–45, 2000
18. Dorai H, Sampath TK: Bone morphogenetic protein-7 modulates genes that maintain the vascular smooth muscle cell phenotype in culture. *J Bone Joint Surg Am* 83 (Suppl 1): S70–S78, 2001
19. Newby AC, Zaltsman AB: Molecular mechanisms in intimal hyperplasia. *J Pathol* 190: 300–309, 2000
20. Schwab SJ, Harrington JT, Singh A, Roher R, Shohaib SA, Perrone RD, Meyer K, Beasley D: Vascular access for hemodialysis. *Kidney Int* 55: 2078–2090, 1999
21. Lundell A, Lindblad B, Bergqvist D, Hansen F: Femoropopliteal-crural graft patency is improved by an intensive surveillance program: A prospective randomized study. *J Vasc Surg* 21: 26–33, 1995
22. Lemson MS, Tordoir JH, Daemen MJ, Kitslaar PJ: Intimal hyperplasia in vascular grafts. *Eur J Vasc Endovasc Surg* 19: 336–350, 2000
23. Nwasokwa ON: Coronary artery bypass graft disease. *Ann Intern Med* 123: 528–545, 1995
24. Osaka S, Osawa H, Miyazawa M, Honda J: Immediate and long-term results of coronary artery bypass operation in hemodialysis patients. *Artif Organs* 25: 252–255, 2001

25. Herzog CA, Ma JZ, Collins AJ: Long-term outcome of dialysis patients in the United States with coronary revascularization procedures. *Kidney Int* 56: 324–332, 1999
26. Liaw L, Almeida M, Hart CE, Schwartz SM, Giachelli CM: Osteopontin promotes vascular cell adhesion and spreading and is chemotactic for smooth muscle cells in vitro. *Circ Res* 74: 214–224, 1994
27. Yue TL, McKenna PJ, Ohlstein EH, Farach-Carson MC, Butler WT, Johanson K, McDevitt P, Feuerstein GZ, Stadel JM: Osteopontin-stimulated vascular smooth muscle cell migration is mediated by beta 3 integrin. *Exp Cell Res* 214: 459–464, 1994
28. Liaw L, Skinner MP, Raines EW, Ross R, Cheresh DA, Schwartz SM, Giachelli CM: The adhesive and migratory effects of osteopontin are mediated via distinct cell surface integrins. Role of alpha v beta 3 in smooth muscle cell migration to osteopontin in vitro. *J Clin Invest* 95: 713–724, 1995
29. Massy ZA, Ivanovski O, Nguyen-Khoa T, Angulo J, Szumilak D, Mothu N, Phan O, Daudon M, Lacour B, Drueke TB, Muntzel M: Uremia accelerates both atherosclerosis and arterial calcification in apolipoprotein E knockout mice. *J Am Soc Nephrol* 16: 109–116, 2005
30. Buzello M, Tornig J, Faulhaber J, Ehmke H, Ritz E, Amann K: The apolipoprotein e knockout mouse: A model documenting accelerated atherogenesis in uremia. *J Am Soc Nephrol* 14: 311–316, 2003
31. Mathew S, Lund RJ, Strebeck F, Tustison KS, Geurs T, Hruska KA: Reversal of the adynamic bone disorder and decreased vascular calcification in chronic kidney disease by sevelamer carbonate therapy. *J Am Soc Nephrol* 18: 122–130, 2007
32. Mathew S, Tustison KS, Sugatani T, Chaudhary LR, Rifas L, Hruska KA: The mechanism of phosphorus as a cardiovascular risk factor in CKD. *J Am Soc Nephrol* 19: 1092–1105, 2008
33. Davies MR, Lund RJ, Mathew S, Hruska KA: Low turnover osteodystrophy and vascular calcification are amenable to skeletal anabolism in an animal model of chronic kidney disease and the metabolic syndrome. *J Am Soc Nephrol* 16: 917–928, 2005
34. Davies MR, Lund RJ, Hruska KA: BMP-7 is an efficacious treatment of vascular calcification in a murine model of atherosclerosis and chronic renal failure. *J Am Soc Nephrol* 14: 1559–1567, 2003
35. Mathew S, Geurs T, Hruska KA: Bone morphogenetic protein-7 inhibits vascular calcification by stimulating the contractile vascular smooth muscle cell phenotype [Abstract]. *J Am Soc Nephrol* 16: 52A, 2005
36. Okabe M, Ikawa M, Kominami K, Nakanishi T, Nishimune Y: 'Green mice' as a source of ubiquitous green cells. *FEBS Lett* 407: 313–319, 1997
37. Leidenfrost JE, Khan MF, Boc KP, Villa BR, Collins ET, Parks WC, Abendschein DR, Choi ET: A model of primary atherosclerosis and post-angioplasty restenosis in mice. *Am J Pathol* 163: 773–778, 2003
38. Eitzman DT, Westrick RJ, Nabel EG, Ginsburg D: Plasminogen activator inhibitor-1 and vitronectin promote vascular thrombosis in mice. *Blood* 95: 577–580, 2000
39. Vicente CP, He L, Pavao MS, Tollefsen DM: Antithrombotic activity of dermatan sulfate in heparin cofactor II-deficient mice. *Blood* 104: 3965–3970, 2004
40. Filippov S, Koenig GC, Chun TH, Hotary KB, Ota I, Bugge TH, Roberts JD, Fay WP, Birkedal-Hansen H, Holmbeck K, Sabeh F, Allen ED, Weiss SJ: MT1-matrix metalloproteinase directs arterial wall invasion and neointima formation by vascular smooth muscle cells. *J Exp Med* 202: 663–671, 2005

Supplemental information for this article is available online at http://www.jasn.org/.